Coherence Histogram Based Wi-Fi Passive Human Detection Approach

Zengshan Tian(✉), Xiaoya Zhang, and Lingxia Li

School of Communication and Information Engineering, Chongqing University of Posts and Telecommunications, Chongqing 400065, China
1159824866@qq.com

Abstract. Some traditional Wi-Fi indoor passive human detection systems only extract the coarse-grained statistical information such as the variance, which leads to low detection accuracy and poor adaptability. To solve the problem, we propose a new coherence histogram for Wi-Fi indoor passive people detection. In the histogram construction process, the method leverages time continuity relationship between received signal strength (RSS) measurements. The coherence histogram captures not only the occurrence probability of signals but also the time relationship between adjacent measurements. Compared to statistical features, the coherence histogram has more effective fine-grained information. The feature vector consists of coherence histograms is used to train the classifier. To eliminate the position drift problem, the Allen time logic helps to establish the transfer relationship between the sub-areas, we correct the results to improve the location accuracy. Compared with the classic passive human detection technology, the F1-measure is improved by nearly 5%.

Keywords: Wi-Fi · Passive human detection · Coherence histogram

1 Introduction

Nowadays, the device-free human detection system has been rapidly developed, such as ultra-wideband radar [1], computer vision [2], sensor networks [3] and radio tomography [4], which can achieve real-time human detection. However, in daily application scene, ultra-wideband radar requires special hardware support, which limits the application range; the monitoring environment under conditions of smoke, lowlight, etc., computer vision fails to detect people accurately, and the technology also has great limitation in smart home which involves privacy issues of users; sensor networks and radio tomography both require to deploy high-density tags, it is difficult for those systems to be used widely in the commercial market due to the expensive equipment costs. As wireless is widely deployed in our daily life, people are almost inseparable from the wireless. The study found

Supported by organization x.

H. Gao et al. (Eds.): ChinaCom 2019, LNICST 313, pp. 95–109, 2020.
https://doi.org/10.1007/978-3-030-41117-6_9

that in the wireless environment, the appearance and movement of the human body can absorb, reflect and diffract part of the signal energy [5]. Using the characteristics of the wireless signal, received signal strength (RSS) based Wi-Fi passive people detection technology became a research hotspot. The technology does not require additional detection equipment carried by people. The characteristics of wide coverage, easy deployment, and low cost are helpful to applicate in the public safety field, commercial field, etc.

2 Related Work

The researchers conducted a variety of research on the original signal to extract the disturbance information. There are three typical detection methods: first of all, the statistical characteristics based system such as moving average (MA) [6] and moving variance (MV) [7] can obtain higher detection performance in a short time, but as time goes by and the environment changes, the performance gradually decreases. Secondly, the researchers have established systems such as RASID [8] and Ichnaea [9] by setting an environment anomaly index. The advantages of the system are efficient and fast when utilizing a single-link to detect the target. However, in the multi-link joint detection, due to the difference between links, it is necessary to adjust the abnormality index of each link to achieve better performance, which increases the system workload.

To solve the above problems, the support vector machine (SVM) [10] based on pattern recognition extracts the statistical features of the signal, such as variance, mean, extreme value, etc. However, the statistical features only reflect the coarse-grained information of the original signal. In contrast, if we use the distribution of the signal to characterize continuous RSS values, we must get more comprehensive and effective information than statistical features. For the people detection problem, wireless links react differently to environment condition, we should make full use of the received signal strength values to independently estimate the distribution of each wireless link in the monitoring environment, so a lightweight and efficient method must be used to find such a distribution. The histogram [11] meets the above requirements. It can estimate the probability distribution and reflect the fluctuation of continuous variables. Although the histogram can reflect the distribution of the signal, the ability of the histogram to obtain data time information is insufficient. Since the time relationship between RSS measurements is useful, the system adds it to the process of the histogram construction. We propose a Wi-Fi passive human detection approach based on coherence histogram.

3 Coherence Histogram Based Detection System

3.1 System Overview

The system overview of the proposed Wi-Fi passive people detection system is shown in Fig. 1. The system consists of three phases: signal collection and processing phase, model training phase and real-time detection phase.

(1) Signal collection and processing
We place some wireless access points (APs) and monitoring points (MPs) in the monitoring area. Secondly, the monitoring area is divided into several sub-areas, the MPs collect RSS measurements when the monitoring area with people and area without people, respectively. Finally, the RSS measurements will be filtered and normalized.
(2) Model training
To characterize all RSS streams received by MPs under different location status of people, the system constructs the coherence histogram for each link and merges them to form the feature vector. Then, the softmax classification model is trained by the feature vector to identify the movement and location of people.
(3) Real-time detection
The classification model classifies the RSS measurements received by the MPs. After that, the Allen-time logic is used to establish the transfer relationship of people movement in sub-areas. At last, the system outputs the final location result that is corrected by the transfer relationship.

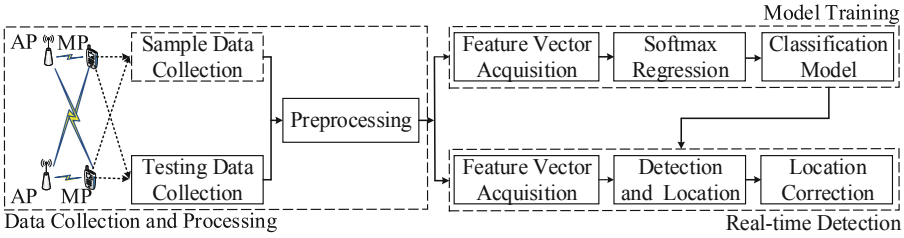

Fig. 1. System model.

3.2 Signal Collection and Processing

In the monitoring area, the number of placed AP and MP is X and Y, respectively. Altogether $J = X \times Y$ wireless links traveling through the monitoring area. The RSS measurements set of the $jth(= 1, 2, \cdots, J)$ wireless link is $RSS^j = [R_1^j, R_2^j, \cdots, R_K^j]$, where R_k^j indicates the kth RSS measurements. Since the noise in the monitoring environment affects the construction of the feature vector, the paper draws on the idea of outlier detection method [12] to design a filter to eliminate those extreme RSS measurements. For every link j, the mean D^j of the RSS^j is determined by

$$D^j = \frac{\sum_{k=1}^{K} R_k^j}{K} \tag{1}$$

and the maximum effective distance B^j from the mean is calculated as follows

$$B^j = 4\sqrt{\frac{\sum_{k=1}^{K} \left(R_k^j - D^j\right)^2}{K}} \tag{2}$$

The filtered outcome $\hat{R}_k^j(k = 1, 2, \cdots, K)$ of R_k^j is obtained by

$$\hat{R}_k^j = \begin{cases} D^j + B^j, R_k^j > D^j + B^j \\ D^j - B^j, R_k^j < D^j - B^j \\ R_k^j, \quad otherwise \end{cases} \tag{3}$$

After filtering all values in the RSS^j, we can get $R\hat{S}S^j = [\hat{R}_1^j, \hat{R}_2^j, \cdots, \hat{R}_K^j]$.

Because the signal distribution needs to be consistent during the construction process of the signal coherence histogram, the filtered $R\hat{S}S^j$ is normalized as $R\tilde{S}S^j = [\tilde{R}_1^j, \tilde{R}_2^j, \cdots, \tilde{R}_k^j]$, where $\tilde{R}_k^j = (\hat{R}_k^j - \hat{R}_{min}^j)\big/(\hat{R}_{max}^j - \hat{R}_{min}^j)$, $\hat{R}_{max}^j$ and $\hat{R}_{min}^j$ are the maximum and minimum values of $R\hat{S}S^j$, respectively.

3.3 Model Training

3.3.1 Feature Vector Construction

Figure 2 shows the fluctuation of the MP-side RSS signal of three wireless links when the monitoring area with people and without people. The wireless link RSS measurements change over a wide range. Therefore, it is possible to judge whether there are people in the monitoring area based on the fluctuation condition of the MP-side RSS signal.

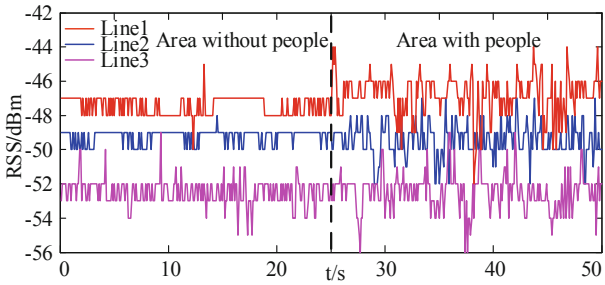

Fig. 2. Fluctuation of three wireless links.

The variance and histogram of three wireless links RSS measurements are shown in Figs. 3 and 4, respectively. From Fig. 3, we see the variance can characterize data features, but the expression is not obvious. Although histogram has a better ability to represent signal features than variance, signal information extracted by histogram is incomprehensive. This paper fully uses the time information of RSS measurements and constructs the coherence histogram.

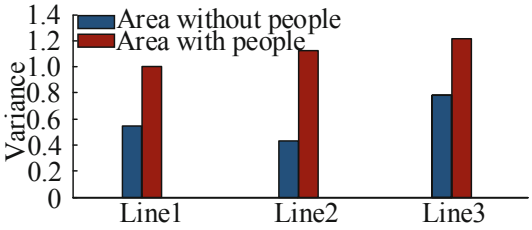

Fig. 3. RSS variances of three links.

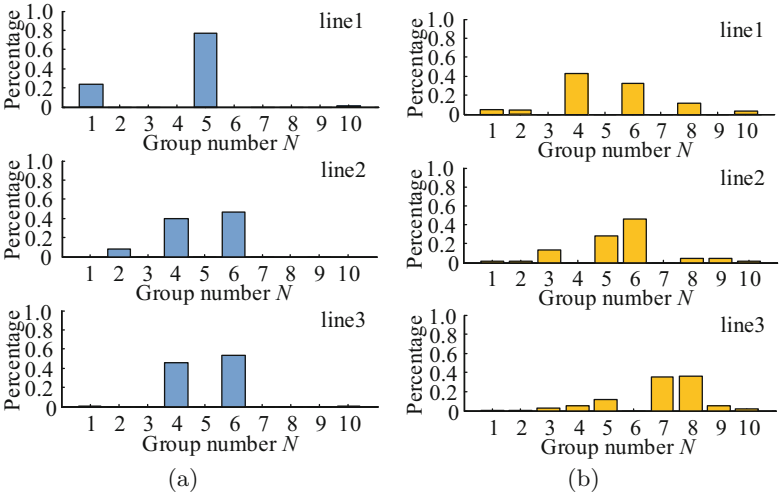

Fig. 4. RSS histograms of three links in different state of the monitoring area. (a) Area without people. (b) Area with people.

We divide $R\tilde{S}S^j$ into N groups of equal length. For the proceed RSS measurements of a link, if there no less than c consecutive measurements falling into the *nth* group, then we say the RSS measurements that belong to the same group are the c coherence, where c is termed as the degree of coherence. Then, the total number of RSS measurements in the *nth* group that meets the coherence degree requirement is recorded as s_n. Finally, the height of the *nth* group $\hat{s}_n^c$ is defined as

$$\hat{s}_n^c = \frac{s_n}{K} \tag{4}$$

where K is the total number of RSS measurements. Based on that, the coherence histogram of the *jth* link is calculated as $\hat{H}^j = [\hat{s}_1^c, ..., \hat{s}_n^c, ..., \hat{s}_N^c]$, where $n = 1, ..., N$. When the degree of coherence $c = 1$, we observe that the traditional histogram is a special case of coherence histogram.

Coherence histograms of three wireless links are shown in Fig. 5. The degree c of coherence directly reflects the change condition of RSS measurements, which

means the more continuous the time of RSS measurements of the same group is, the bigger the group height is. It reflects that the change speed of the signal is slow in a short time and the signal fluctuation is stable.

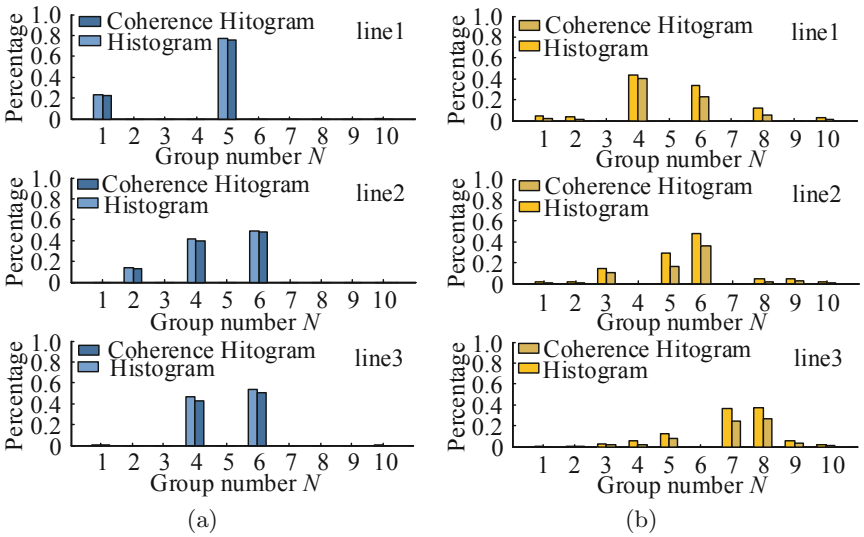

Fig. 5. RSS coherence histograms of three links in different state of the monitoring area. (a) Area without people. (b) Area with people.

To meet the real-time needs of the detection system, the entire samples should be divided into smaller samples. The sliding window mechanism [7] of length L divides different location status data. Samples of each location status of people are both $I = \lceil (K - L)/f \rceil$ for every wireless link, where f is the sampling frequency. There are total M kinds of samples in every sub-area and one type of sample corresponds to one location status. The coherence histogram of the *ith* samples of link j is calculated as $\hat{H}^j_{m,i} = [\hat{s}^c_{m,1}, \cdots, \hat{s}^c_{m,n}, \cdots, \hat{s}^c_{m,N}]$, $m = 1, \cdots, M$, $i = 1, \cdots, I$.

With the coherence histogram of all wireless links for every sub-area, the feature vector $F^i_{m,a}$ is formed by merging them

$$F^i_{m,a} = [\hat{H}^1_{m,i}, ..., \hat{H}^j_{m,i}, ..., \hat{H}^J_{m,i}]^T \tag{5}$$

where a denotes the sub-area number. The feature vector $F^i_{m,a}$ is a $NJ \times 1$ vector and the feature map is built as follows

$$\Lambda = \left\{ F^i_{m,a} | a = 1, ..., A; m = 1, ..., M; i = 1, ..., I \right\} \tag{6}$$

3.3.2 Classification Model Construction

The paper trains the classification model based on the feature vector $F^i_{m,a}$ of each location status samples to classify the RSS measurements in real-time

detection phase. Let I be the number of classifiers, for the ith classifier, the training process is as follows.

In the real-time detection phase, the RSSt denotes the tested RSS measurements whose feature vector is F, the detection problem can be formulated as the following minimization problem

$$(\hat{m}, \hat{a}) = \arg\min_{m,a} \left\| F - F^i_{m,a} \right\| \tag{7}$$

where $\hat{m}$ and $\hat{a}$ are the estimated index of status and location of the target, respectively.

The monitoring area is divided into A sub-areas and each sub-area has M possible states. Therefore, there are total $Q = M \times A$ types of location states and RSSt can be any one of them, it is a typical multiple classes problem. This paper utilizes the softmax regression method which can convert the input feature vector into a probability [13]. As is shown in Fig. 6, the softmax regression model converts the input feature vector of every class into a probability $p(y_{m,a} = r|F^i_{m,a}, \theta)$ for $r = 1, ..., Q$. That is, it estimates the output probability of the class label y taking on Q classes.

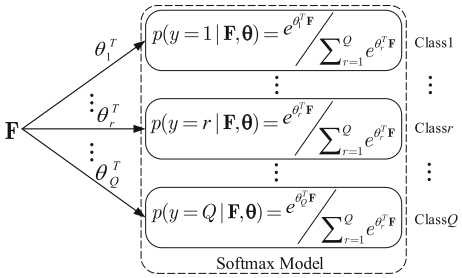

Fig. 6. Softmax regression model.

The output of the softmax regression model formulates as follows

$$h(F^i_{m,a}) = \begin{bmatrix} p(y_{m,a} = 1|F^i_{m,a}, \theta) \\ \vdots \\ p(y_{m,a} = r|F^i_{m,a}, \theta) \\ \vdots \\ p(y_{m,a} = Q|F^i_{m,a}, \theta) \end{bmatrix} = \frac{1}{\sum_{r=1}^{Q} e^{\theta_r^T F^i_{m,a}}} \begin{bmatrix} e^{\theta_1^T F^i_{m,a}} \\ \vdots \\ e^{\theta_r^T F^i_{m,a}} \\ \vdots \\ e^{\theta_Q^T F^i_{m,a}} \end{bmatrix} \tag{8}$$

where θ_r is a $NJ \times 1$ vector that indicates the model parameter for the rth output. All the system parameters of regression model are recorded as $\theta = [\theta_1, \ldots, \theta_Q]^T$, which is a $Q \times NJ$ matrix.

Firstly, the cost function of the regression model is defined as follows

$$\varphi_i(\theta) = -\frac{1}{Q}\left[\sum_{a=1}^{A}\sum_{m=1}^{M}\sum_{r=1}^{Q} 1\{y_{m,a} = r\} \log \frac{\theta_r^T F_{m,a}^i}{\sum_{l=1}^{Q} e^{\theta_l^T F_{m,a}^i}}\right] + \frac{\lambda}{2}\sum_{r=1}^{Q}\sum_{q=1}^{NJ}\theta_{rq}^2 \quad (9)$$

where $1\{\cdot\}$ represents an indicator function. When $y_{m,a} = r$, then $\{y_{m,a} = r\} = 1$, otherwise, $\{y_{m,a} = r\} = 0$. θ_{rq} represents the *rth* row and *qth* column element of the parameter matrix θ and λ is the proportion of the weight decay term.

After that, the cost function $\varphi_i(\theta)$ is strictly convex and its derivative is determined as follows

$$\nabla\theta_r\varphi_i(\theta) = -\frac{1}{Q}\sum_{a=1}^{A}\sum_{m=1}^{M} F_{m,a}^i[1\{y_{m,a} = r\} - p(y_{m,a} = r|F_{m,a}^i, \theta)] + \beta\theta_r \quad (10)$$

Finally, it is straightforward to solve the parameter matrix θ with the gradient descent algorithm using the feature vectors of training samples.

3.4 Real-Time Detection

3.4.1 Target Detection and Location

In the real-time detection phase, we use the sliding window mechanism that is the same as the data collection and processing phase to get the tested RSS measurements. Then, with the coherence histogram feature vector F extracted from the tested data, the probabilities of location status of people can be calculated as follows

$$h(F) = \theta \times F \quad (11)$$

The classification $(\hat{m}, \hat{a})$ of the element with the largest value in the $Q \times 1$ probability vector $h(F)$ is the current estimated location status of the target.

3.4.2 Physical Connection Relationship Construction

The connection relationship between the actual physical structures can constrain the movement behavior of people, hence, the movement pattern of people in

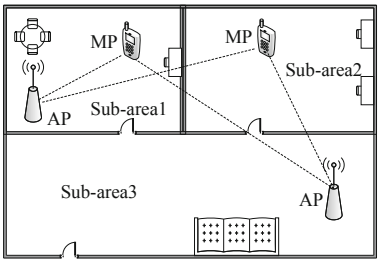

Fig. 7. Division of the monitoring area.

each sub-area is determined with the Allen Time Logic [14]. Figure 7 shows the divided sub-area for the monitoring area and Fig. 8 shows the Allen Time Logic that defines 8 time-order relationships between different events.

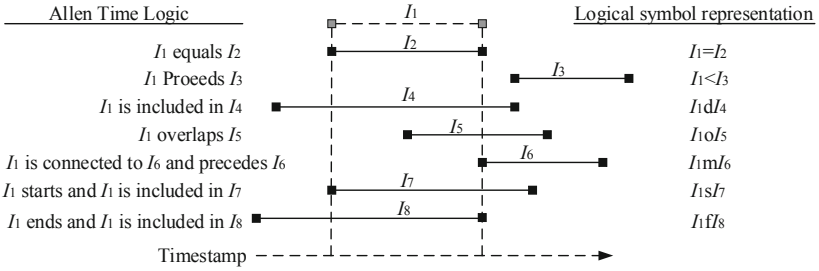

Fig. 8. Allen linear temporal logic.

All the motion modes are obtained by observing human behaviors in the monitoring area, Fig. 9 shows four of them and BP is the breakpoint which separates every event. Based on that, according to the Allen Time Logic, Fig. 10 shows the event map, the nodes represent events and the dotted path is the longest path. In each event graph, there is one and only one longest path, which satisfies two relationships: the first one is the happening order of events and the event nodes are connected by the operator 'm'; the second one is the end of movement and the operator 'f' connects the last event node to the movement node. According to each longest path associated with the sub-areas, the connection relationship of sub-areas can be constructed. Figure 11 shows the movement map that is the physical logic diagram of the monitoring area.

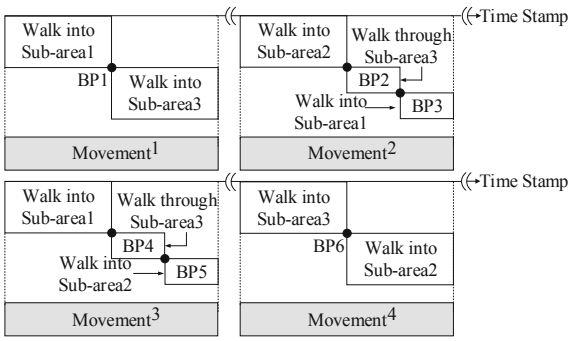

Fig. 9. People movement mode of the monitoring area.

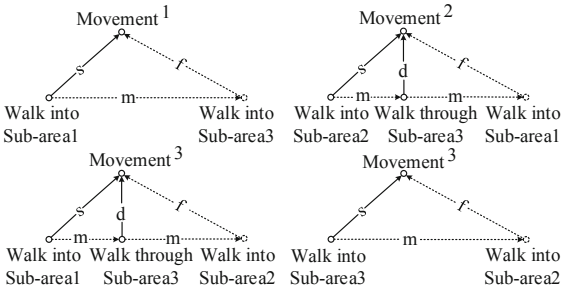

Fig. 10. Event map.

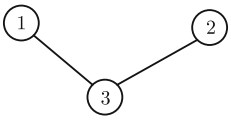

Fig. 11. Movement map.

3.4.3 Sub-area Transfer Weight Determination

According to the analysis of people behaviors in paper [15], the pedestrian movement rate distribution is shown in Table 1. This paper explores the distribution of actual walking distances of people during the sampling interval and uses the information to determine the transfer weight of sub-areas. Let d_{ab}^{min} and d_{ab}^{max} represent the minimum and maximum walking distance from sub-area a to sub-area b (a and b can be the same sub-area), respectively. The transfer probability W_{ab} from a to b is calculated by the cumulative distribution function (CDF)

$$\begin{aligned} f(v) &= \begin{cases} \frac{1}{\sigma\sqrt{2\pi}} \exp\left(-\frac{(v-\mu)^2}{2\sigma^2}\right) & v_{\min} \le v \le v_{\max} \\ 0 & \text{otherwise} \end{cases} \\ W_{ab} &= \int_{d_{ab}^{\min}}^{d_{ab}^{\max}} f(v) \cdot t dv \end{aligned} \tag{12}$$

where μ and σ are the mean and variance of pedestrian movement rate. Then, we normalize the W_{ab} and get $\tilde{W}_{ab} = W_{ab} / \sum_{b=1}^{A} W_{ab}$.

Table 1. Pedestrian movement rate law.

Mean velocity (m/s)	Standard deviation (m/s)	Minimum (m/s)	Maximum (m/s)
1.127	0.5324	0.007	2.499

3.4.4 Location Correction

Since the motion state of people is continuous, the sliding window mechanism with the length G is used to filter the location at the current moment.

The transferred score that the target walks from the location obtained in the previous second to each location in the window is calculated as follows

$$Q_{ab} = n_b \times \tilde{W}_{ab} \tag{13}$$

where $n_b(\sum n_b = G)$ is the number of sub-area b in the window and $\tilde{W}_{ab}$ is the transition probability of sub-area a to sub-area b. In the end, the filtered result of the target location corresponds to the sub-area b when the score is the largest.

4 Experiment Evaluation

4.1 Experiment Setting

The layout of the experimental scene is shown in Fig. 12, we establish a prototype network to evaluate the performance of the proposed scheme in a typical complex home scene. The indoor area is 59.48 m^2. Considering the limited number of available access points (APs) in the actual indoor environment, the network consists of 5 nodes, node 1 (Huawei Honor Router, WS851) is the access point that coordinates the operation of the network, while nodes 2 to 5 are the monitoring points (Samsung Mobile Phones, GT-S7568) that collect RSS measurements. A total of 4 wireless links cover the monitoring area. The AP uses the transmission over the frequency of 2.45 GHz and the sampling frequency of the MP is 10 Hz. MPs collect RSS measurements of all location states of people and the collection time for each kind of sample is 10 min. After that, the system performs multiple tests and each test lasts 5 min. According to the received RSS measurements, the system determines the location status of the target uniquely. The default parameters of the system are summarized in Table 2.

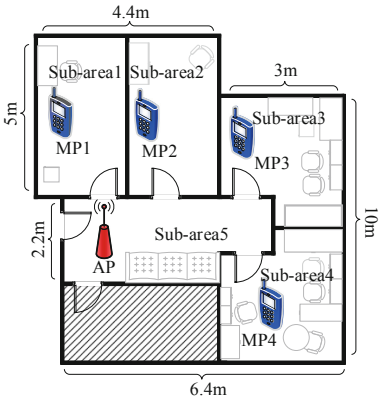

Fig. 12. Experimental scene.

Table 2. System default parameter values.

Parameter	Default value	Meaning
L	10	Sliding window size
N	5	Group number
C	3	Coherence degree
G	5	Filter window size

4.2 Parameter L, N and C for System Performance

As is shown in Fig. 13, when the L is restively short, the insufficient number of samples leads to the lack of discrimination of the feature vector, which makes the system performance is bad; however, when the L is restively long, due to the continuity of the movement of the target, there are lots of previous RSS measurements in the window. If the location status of the target changes at the current time, the previous data may cause misjudgment of the system. When the L is 20 or 30, the overall system performance is excellent, but considering the real-time needs of the system, we choose $L = 20$.

The next step is to confirm the influence caused by N and C on the system performance. In Fig. 13, we can see that relatively smaller C leads to the RSS values time continuity requirement is extremely low. A large number of motion RSS measurements fall into the same group due to the insufficient number of groups N. Hence, both of them can cause the inaccuracy judgment of motion status. In contrast, the restively larger C or the excessive N can result in misjudgment when there is no target walking around the monitoring area. Therefore, this paper chooses $L = 20$, $N = 10$, $C = 4$.

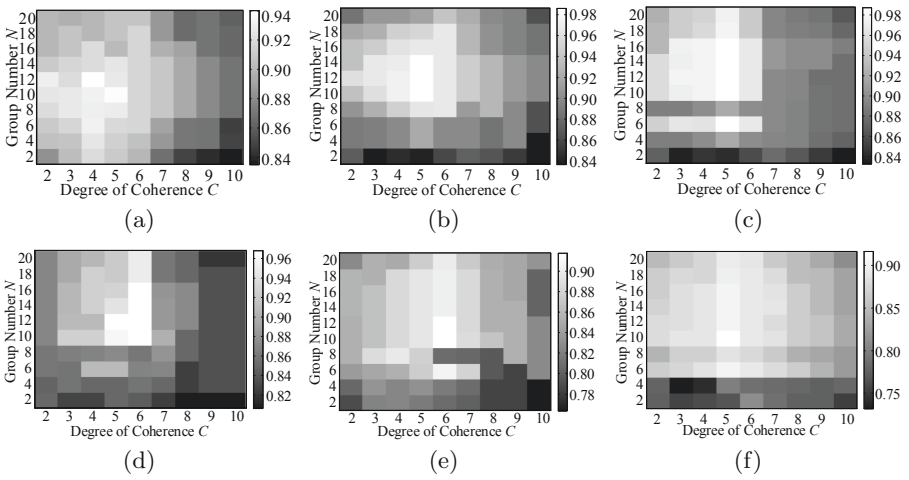

Fig. 13. F1-measure of different parameter. (a) $L = 10$. (b) $L = 20$. (c) $L = 30$. (d) $L = 40$. (e) $L = 50$. (f) $L = 60$.

4.3 Parameter G for System Performance

The sub-area location accuracy and average location accuracy are shown in Figs. 14 and 15, respectively. As we can see, the sub-area location accuracy increases as the filter window size increases, but when the window size reaches a certain size, the extension of the G makes the location accuracy decrease. Combining the results of the two graphs, the selection of the G is preferably between 5 and 10. The filter window $G = 10$ in this paper.

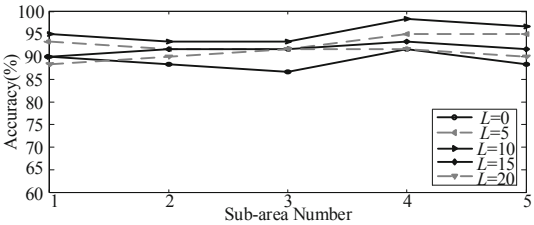

Fig. 14. Location accuracy.

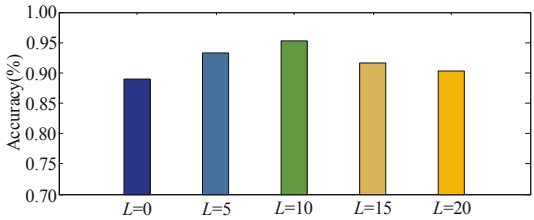

Fig. 15. Average location accuracy.

4.4 Performance Analysis

This section compares the proposed method with the MV system, the MA system, the histogram-based system, and the RASID system, the results are shown in Table 3. It can be seen that the F1-measure can reach 98%, the false positive rate (FP) and the false negative rate (FN) of the proposed algorithm are much lower. The confusion matrix is shown in Fig. 16, we can see the location accuracy is significantly improved after being filtered. As is shown in Fig. 17, filtered location accuracy of the detected target is at least 92%, the performance is higher than both Inchead system and Multi-feature PNN system [16]. To sum up, the proposed system has obvious advantages in the field of passive people detection.

Table 3. Comparison of detection performance with existing detection technologies.

Performance	MA	MV	RASID	Histogram	Coherence histogram
FN	0.1042	0.1174	0.0498	0.0687	0.0361
FP	0.1352	0.0962	0.0652	0.0997	0.0106
F1-measure	0.8799	0.8952	0.9303	0.9145	0.9769

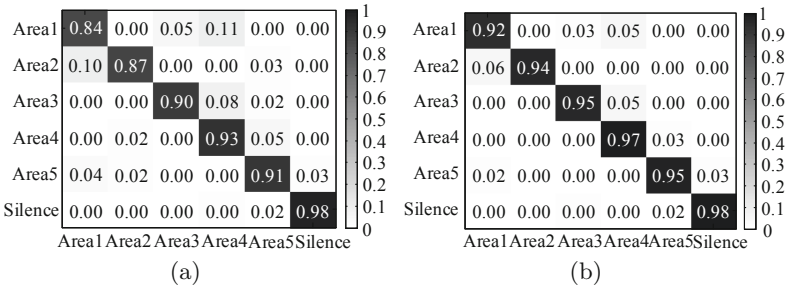

Fig. 16. Confusion matrix of location. (a) Initial location result. (b) Filtered location result.

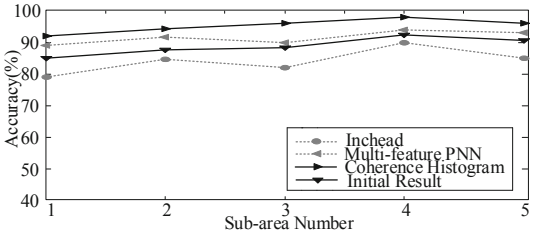

Fig. 17. Comparison with existing locating technology.

5 Conclusion

To detect and locate people in an indoor environment, this paper proposes a people detection approach based on coherence histogram after comprehensively analyzing the advantages and disadvantages of the variance and histogram that are used to represent the original signal characteristics. On the one hand, the coherence histogram contains more fine-grained information which is related to the time relationship of RSS measurements. Therefore, the classification accuracy rate is been effectively improved. On the other hand, the proposed system has excellent tracking performance because the transfer relationship between different sub-areas is helpful to correct the location results. Therefore, the proposed method has more excellent performance.

References

1. Daim, T.J., Lee, R.M.A.: Indoor environment device-free wireless positioning using IR-UWB Radar. In: 2018 IEEE International Conference on Artificial Intelligence in Engineering and Technology (IICAIET), pp. 1–4. IEEE, Kota Kinabalu (2018)
2. Yasar, F.G., Kusetogullari, H.: Underwater human body detection using computer vision algorithms. In: 2018 26th Signal Processing and Communications Applications Conference (SIU), pp. 1–4. IEEE, Izmir (2018)
3. Wang, Q., Yiğitler, H., Jäntti, R., Huang, X.: Localizing multiple objects using radio tomographic imaging technology. IEEE Trans. Veh. Technol. **65**(5), 3641–3656 (2016)
4. Alippi, C., Bocca, M., Bopacchi, G., Patwari, N., Roveri, M.: RTI Goes Wild: radio tomographic imaging for outdoor people detection and localization. IEEE Trans. Mob. Comput. **15**(10), 3641–3656 (2016)
5. Pirzada, N., Nayan, M., Hassan, M., Subhan, F.: Filters for device-free indoor localization system based on RSSI measurement. In: 2014 International Conference on Computer and Information Sciences (ICCOINS), pp. 1–5. IEEE, Kuala Lumpur (2014)
6. Lv, J.G., Yang, W., Man, D.P., Du, X.J.: Wii: device-Free passive identity identification via WiFi signals. In: 2017 IEEE Global Communications Conference, pp. 1–6. IEEE, Singapore (2017)
7. Youssef, M., Moussa, M., Agrawala, A.: Challenges: device-free passive localization for wireless environments. In: Proceedings of the 13th Annual International Conference on Mobile Computing and Networking, pp. 222–229. ACM, Canada (2007)
8. Kosba, A.E., Saeed, A., Youssef, M.: RASID: a robust WLAN device-free passive motion detection system. In: 2012 IEEE International Conference on Pervasive Computing and Communications, pp. 180–189. IEEE, Lugano (2012)
9. Saeed, A., Kosba, A.E., Youssef, M.: Ichnaea: a low-overhead robust WLAN device-free passive localization system. IEEE J. Sel. Top. Sig. Process. **8**(5), 5–15 (2014)
10. Ilao, J., Cordel, M.: Crowd estimation using region-specific HOG With SVM. In: 2018 15th International Joint Conference on Computer Science and Software Engineering (JCSSE), pp. 1–5. IEEE, Nakhonpathon (2012)
11. Koray, K.: Histogram-based contextual classification of SAR images. IEEE Geosci. Remote Sens. Lett. **12**(1), 33–37 (2014)
12. Han, J., Kamber, M., Pei, J.: Data Mining Concepts and Techniques, 3rd edn. Elsevier, Amsterdam (1999)
13. Heckerman, D., Meek, C.: Models and selection criteria for regression and classification. In: 13th Conference on Uncertainty in Artificial Intelligence (UAI), pp. 223–228. Morgan Kaufmann, San Francisco (2009)
14. Roşu, G., Bensalem, S.: Allen linear (interval) temporal logic – translation to LTL and monitor synthesis. In: Ball, T., Jones, R.B. (eds.) CAV 2006. LNCS, vol. 4144, pp. 263–277. Springer, Heidelberg (2006). https://doi.org/10.1007/11817963_25
15. Azevedo, T.S., Bezerra, R.L., Campos, A.V.C., Moraes de, L.F.M.: An analysis of human mobility using real traces. In: 2009 IEEE Wireless Communications and Networking Conference, pp. 1–6. IEEE, Budapest (2009)
16. Tian, Z.S., Zhou, X.D., Zhou, M., Li, S.S.: Indoor device-free passive localization for intrusion detection using multi-feature PNN. In: 2015 10th International Conference on Communications and Networking in China (ChinaCom), pp. 272–277. IEEE, Shanghai (2015)